Asian Journal of Chemistry; Vol. 37, No. 9 (2025), 2123-2134
ASIAN JOURNAL OF CHEMISTRY
https://doi.org/10.14233/ajchem.2025.33944

Synthesis, Spectral Characterization, Density Functional Theory Studies and Antidiabetic Activities of Copper(II) Complexes of Schiff Bases Derived from N-Benzoyl Glycylhydrazide

SAPAM SAYA DEVI[1], RODI LAISHRAM[1], AMAR NINGTHOUJAM[1], SOUBAM SOMANANDA MEETEI[1], S. SURESHKUMAR SINGH[2] and RAJKUMARI LONIBALA[1,*]

[1]Department of Chemistry, Manipur University, Canchipur-795003, India
[2]Department of Botany, Manipur University, Canchipur-795003, India

*Corresponding author: E-mail: lonibala@manipuruniv.ac.in

Received: 28 April 2025 *Accepted*: 30 June 2025 *Published online*: 30 August 2025 AJC-22091

Two new Schiff bases, (*E*)-N-(2-(2-(2-hydroxy-3-methoxybenzylidene)hydrazineyl)-2-oxyethyl)benzylidene)hydrazineyl)-2-oxyethyl)-benzamide (H_2L^1), (*E*)-N-(2-((2-hydroxynapthalen-1-yl)methylene)hydrazineyl)-2-oxyethyl)benzamide (H_2L^2) and their Cu(II) complexes were synthesized and characterized by elemental analyses, molar conductance, thermal analysis, magnetic susceptibility, UV-Vis, IR, EPR and mass spectroscopic data. Formation of Cu(II) complexes having 1:1 metal: ligand stoichiometry was ascertained from the elemental and thermogravemetric analyses. The observed magnetic moment is consistent with the expected value for Cu(II) (d^9) complexes, which typically exhibit one unpaired electron. Spectral and DFT studies suggest pentacoordinated geometries for the complexes in which the ligands act as a tridentate species bonding through the carbonyl-O, azomethine-N and phenolate/phenolic-O. The molecular geometries of the complexes were thoroughly optimized using the Global Hybrid Minnesota functional M06, with the Pople 6-31+G(d,p) basis set for oxygen and nitrogen and the Def2-SVP basis set for hydrogen, carbon and heavy transition metal copper atom in the DFT calculations to improve the balance between accuracy and computational cost. The antidiabetic properties of the ligands and their Cu(II) complexes were investigated, revealing that the complexes exhibited significant enzyme inhibition activity.

Keywords: Schiff bases, Copper ion, Pentacoordinated, Tridentate, DFT studies, Antidiabetic activities.

INTRODUCTION

Schiff bases are considered 'privileged ligands' due to their ability to coordinate with a wide range of metal ions and stabilize various oxidation states under favorable conditions [1]. They represent a significant class of compounds in organic chemistry, known for their thermal and chemical stability, which enables them to maintain performance under high temperatures and pressures. Their synthetic versatility, strong coordination ability, structural similarity to the biological molecules and the presence of imine (-N=CH-) functional groups have made them a subject of extensive investigation in coordination chemistry and related fields [2-4].

Owing to their excellent chelating abilities, Schiff bases play a vital role in coordination chemistry by readily forming stable complexes with a wide range of metal ions. Their metal complexes have a significant role in the branch of analytical and coordination chemistry [5,6] and also considerable importance in pharmaceutical and biological fields like antitumor [7,8] antimicrobial [9-11], anti-inflammatory actions, antitubercular [12], antibacterial, antidiabetic and antioxidant [13-15]. These complexes have been extensively studied in an effort to create new, potent medications and show a likely correlation between chemical structure and biological action [16,17]. Schiff bases and their complexes are also used as probes for ion detection in chemistry, environment, biology and other fields [18-21]. With the presence of an azomethine (-C=N-N-C-) moiety, Schiff bases display multidentate ligand properties and have the ability to settle down metal ions with different oxidation numbers and can produce different types of molecular geometries [22-25].

Amino acids and their derivatives can serve as an important building block for a number of important organic ligands in general and as the amine component in the synthesis of Schiff bases, in particular [26]. Amongst the amino acid derivatives, N-protected amino acids are important in that the

introduction of a substituent such as acetyl, benzoyl or benzylo carbonyl group directly on the amino group, could reduce the ligand field of the in-plane donor thus diminishing the affinity of the amino group for the metal ion and permitting a variety of co-ordinating type. The choice of N-protected amino acid as a precursor in Schiff base ligand synthesis thus offers versatility in tailoring the ligand structure, which can influence the properties and reactivity of the resulting metal complexes. The N-protected group on the amino acid also helps in controlling the reactivity and selectivity of the reaction, ensuring that the Schiff base is formed at the desired site [27,28]. For the last two decades, a number of Schiff bases based on N-benzoyl glycine and their metal complexes have been synthesized in our laboratory [29-32] and their ligational behaviour towards the transition metal ions have been studied. In continuation to earlier work, we now synthesize two new Schiff bases from the interaction of N-benzoyl glycine hydrazide (NBzGH) with 3-methoxy salicylaldehyde and 2-hydroxy-1-naphthaldehyde and their Cu(II) complexes. The metal-ligand stoichiometry, possible geometries, chelation and bonding in the complexes were ascertained on the basis of magnetic measurements, thermal analysis and various spectroscopic studies. DFT studies were also carried out to predict the electronic properties and charges of molecules. HOMO and LUMO energies were calculated since such energy levels play an important role in understanding the reactivity and stability of the molecules [33,34]. Mulliken charges were also computed on the basis of electron density from these calculations. DFT calculations were performed to obtain Hirshfeld and CM5 Charges, which were then analyzed to gain insights into how electrons are distributed and arranged within the molecular system [35]. A comparative analysis involving Mulliken, Hirshfeld and CM5 Charges for both the complexes was also conducted. The ligands and complexes were screened for the antidiabetic properties.

EXPERIMENTAL

2-Hydroxy-1-naphthaldehyde, 3-methoxy salicylaldehyde and N-benzoyl glycine were obtained from Sigma-Aldrich and $CuCl_2 \cdot 4H_2O$ from Merck, USA. All the other chemicals and solvents used in this study were of analytical grade.

Characterization: Copper was estimated iodometrically while chlorine was estimated gravimetrically following standard procedures [36]. Hydrazine contents of the ligands were determined volumetrically by KIO_3 method after subjecting the ligands to acid hydrolysis with 6 N HCl for about 4 h [36]. C, H and N were micro-analyzed using an elemental analyzer Euro-E300. IR spectra were recorded on an IRAffinity-1S FT-IR spectrophotometer Shimadzu in the range of 4000-400 cm^{-1}. An UV-2600, UV-Vis spectrophotometer, Shimadzu was employed to obtain the electronic absorption spectra. Magnetic susceptibility measurements were performed using a Sherwood magnetic susceptibility balanced at room temperature. Thermal analysis was done by using EXSTAR TG/DTA 6300 and the initial weight taken for both complexes is 10 mg each. The conductivity of the complexes was measured in 10^{-3} M DMSO at 25 ºC employing an Eutech Con 510. ESR spectra were recorded on a JEOL, JES-FA 200 ESR Spectrometer, X-band microwave unit using tempol as field maker. Mass spectra were recorded using LC-MS water Alliance e2695/HPLC-TQD Mass spectrometer. ^{1}H NMR for the ligands were measured in NMR 500 MHz Spectrometer, Bruker, Advance III HD. Powder X-ray diffraction (XRD) analyses were performed on PAN analytical X-ray diffractometer (X-Pert Pro).

Antidiabetic studies: The antidiabetic activity of the Schiff base ligands and their Cu(II) complexes was evaluated using an *in vitro* α-glucosidase inhibition assay, following the 96-well microplate-based method described by Kumar *et al*. [37]. In this method, 1 mg of each sample was dissolved in 20 µL each of DMSO, $CHCl_3$, MeOH, water, ethanol and ethyl acetate and then diluted to 1 mL in 2 mL Eppendrof tube with serine water and these samples were employed for enzyme assay. In a reaction, volume of 75 µL, a 96-well microplate was used to conduct the α-glucosidase inhibition experiment. After adding 25 µL of the α-glucosidase enzyme (0.5 U) to the test sample solution (1.0 mg/mL), the mixture was pre-incubated for 10 min at 37 ± 1 ºC. Following the pre-incubation phase, the reaction mixture was incubated at 37 ± 1 ºC for 30 min with 25 µL of substrate (0.5 mM *p*-nitrophenylgluconate, PNPG). For every sample, a blank reaction comprising 25 µL of the test sample, 25 µL of buffer which served as the enzyme substitute and 25 µL of the substrate (0.5 mM PNPG) was added. In addition, a standard medication (acarbose, 1.0 mg/mL) and a control reaction comprising 25 µL buffer with 25 µL of α-glucosidase enzyme and 25 µL of substrate (0.5 mM PNPG) were included for comparison and reference. Every reaction was carried out in triplicate, including the test, blank, control and standards. A 0.2 M sodium carbonate solution containing 100 µL was added to stop the reactions after 30 min. After measuring the absorbance of *p*-nitrophenol (PNP, yellow colour) emitted in the reaction mixtures from PNPG (substrate) as a result of enzyme activity and blank reactions, the percentage of α-glucosidase activity inhibition was calculated by using the formula:

$$\alpha\text{-Glucosidase inhibition (\%)} = \frac{\text{Control OD} - \text{Sample OD}}{\text{Control OD}} \times 100$$

[Control OD = OD of the control reaction without inhibitor-Blank OD; Sample OD = Sample OD – Sample blank OD]. Following the same procedure, the dose-effect relationship of specific compounds that significantly inhibited α-glucosidase activity during the screening assay was calculated. Test sample concentrations of 10, 20, 30, 40 and 50 µg were used, corresponding to 5, 10, 15, 20 and 25 µL of the test sample solutions (1.0 mg/mL, 500 µL reaction volume) and the standard drug acarbose (1.0 mg/mL), respectively. The IC_{50} values of the test samples and standards were calculated using online toolkit for IC_{50} (http://www.ic50.tk) and GraphPad Prism.

Computational details of DFT studies: All the calculations were executed using the Linux version of the Gaussian 16 software suite [38]. The Global hybrid Minnesota functional M06 with 27% HartreeFock exchange was used in the calculations [39]. People's split valence basis set 6-31+G(d,p) [40] with polarization functions are used for oxygen and nitrogen; the split valence polarization basis set of Karlsruhe, Def2-SVP [41,42] is used for hydrogen, carbon and copper atoms. The structure obtained based on the experimental results is used for the DFT calculations. At first, the geometries of

the ligand and Cu(II) complex which have doublet multiplicity were optimized in the ground state which is indicated by the maximum remaining force on all the atoms and their maximum displacement well below the convergence threshold value of 300×10^{-6} and 1200×10^{-6}, respectively. Frequency calculations were performed on the optimized geometries to confirm that the geometries correspond to local minima in a potential surface by the absence of imaginary frequency. All the energies reported here are thermal-free energy corrected electronic energies.

Synthesis of the Schiff base ligands: N-Benzoyl glycylhydrazide (NBzGH) was prepared from N-benzoyl glycine as reported [43] and confirmed from the melting point and spectral data. Schiff base (*E*)-N-(2-(2-(2-hydroxy-3-methoxybenzylidene)hydrazineyl)-2-oxyethyl)benzamide (H_2L^1) and (*E*)-N-(2-(2-((2-hydroxynapthalen-1-yl)methylene)hydrazineyl)-2-oxyethyl)benzamide (H_2L^2) were synthesized by refluxing ethanolic solutions of NBzGH with 3-methoxy salicylaldehyde and 2-hydroxy-1-naphthaldehyde, respectively in the 1:1 molar ratio for 4 h on water bath. The reaction mixtures were filtered and precipitates were obtained on keeping the filtrate overnight (**Scheme-I**). The precipitates were recrystallized, dried in air and characterized by elemental analysis and spectral data.

H_2L^1: Yield: 80 %; m.p.: 190 ºC, Elemental analysis: calcd. (found) of % $C_{17}H_{17}N_3O_4$: C: 62.32 (62.12); H: 5.12 (5.30); N: 12.84 (12.71); N_2H_4: 9.29 (9.70). IR (KBr, ν_{max}, cm^{-1}): 1699 (amide I), 1531(amide II), 1463 (amide III) of hydrazide moiety, 1622 (amide I), 1500 (amide II), 1323 (amide III) of benzamide moiety, 1577 (C=N) and 948 (N-N); ^1H NMR (500 MHz, $CDCl_3$, δ ppm): 9.1 (H, singlet, OH), 3.6 to 4.4 (2H, triplet, CH_2), 7.3-7.5 (8H, multiplets, ring proton), 8.7-8.3 (H, triplet, C_6H_6CONH-) and 7.86 (H, singlet, -NCH). Mass: M+ *m/z* 327.

H_2L^2: Yield: 80 %; m.p.: 181 ºC, Elemental analysis: calcd. (found) of % $C_{20}H_{17}O_3O_3$: C: 62.16 (69.12); H: 4.89 (5.0); N: 12.00 (12.10); N_2H_4: 9.14 (9.22). IR (KBr, ν_{max}, cm^{-1}): 1697 (amide I), 1551 (amide II), 1481 (amide III) of hydrazide moiety, 1637 (amide I), 1521 (amide II), 1411 (amide III) of benzamide moiety, 1575 (C=N) and 989 (N-N); ^1H NMR (500 MHz, $CDCl_3$, δ ppm): 9.6 (H, singlet, OH), 3.6 to 4.4 (2H, triplet, CH_2), 7.2-7.6 (8H, multiplets, ring proton), 7.8 to 8.1 (H, triplet, C_6H_6CONH). Mass: M+ *m/z* 347.

Synthesis of Cu(II) complexes: Ethanolic solutions of 1 mmol of the Schiff base ligands (0.327 g of H_2L^1 in 20 mL ethanol and 0.347 g of H_2L^2 in 20 mL ethanol) were mixed separately each with ethanolic solution of 1 mmol of $CuCl_2 \cdot 4H_2O$ (0.170 g in 20 mL ethanol). The reaction mixtures were refluxed at 80 ºC for 4 h. Upon cooling, the solutions were filtered, and the resulting filtrates were left to stand at room temperature under open conditions. Pale green crystals of complex **1** formed after 72 h, while complex **2** precipitated as olive green solids after 48 h (**Scheme-I**).

RESULTS AND DISCUSSION

Schiff bases, H_2L^1 reacts with $CuCl_2$ in ethanol to form a deprotonated Cu(II) complex, $[Cu(L^1)(H_2O)_2]$ while H_2L^2 forms an adduct having the molecular formula $[Cu(H_2L^2)(H_2O)Cl]Cl$. Table-1 summarizes the colour, analytical and molar conductance data of the Schiff base ligands and their complexes. The elemental data is compatible with complexes having 1:1 metal-ligand stoichiometry. Both the complexes are stable and non-melting up to 230 ºC. Both complexes are soluble in water, MeOH, EtOH, $CHCl_3$, DMSO and ethyl

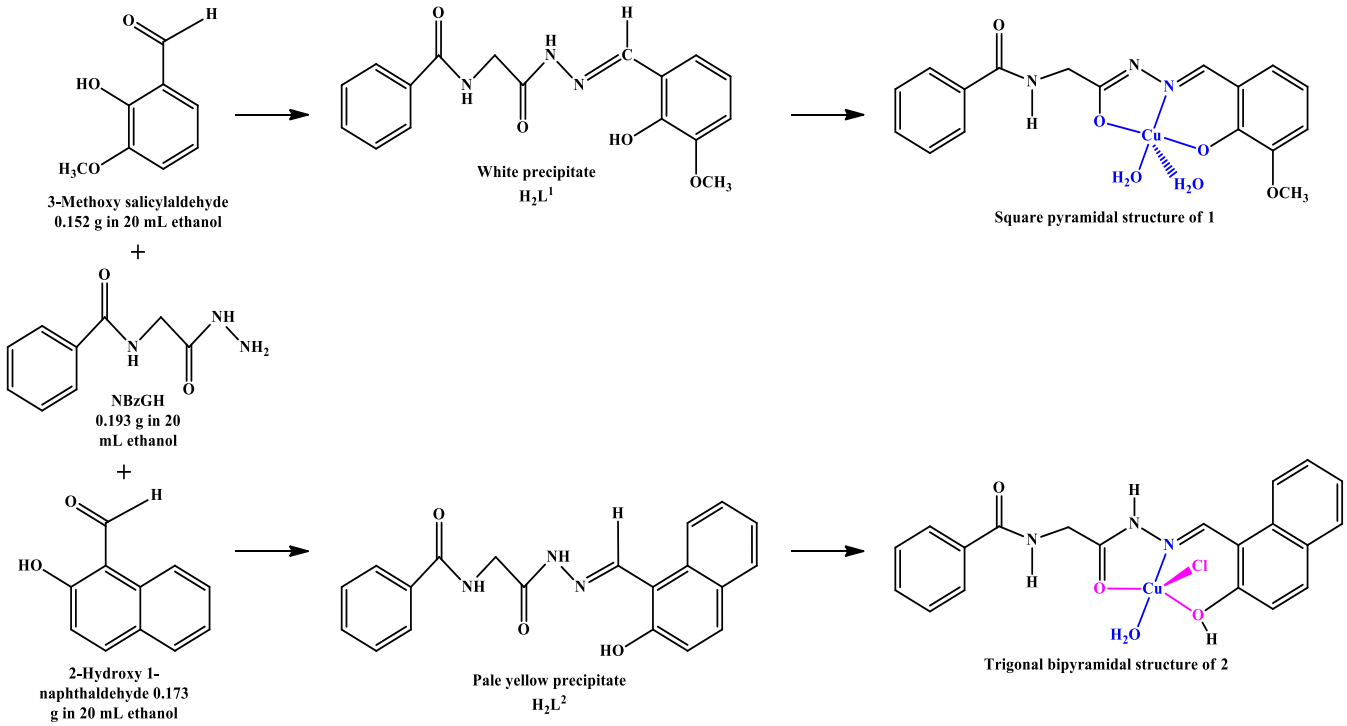

Scheme-I: Synthesis of (*E*)-N-(2-(2-(2-hydroxy-3-methoxybenzylidene)hydrazineyl)-2-oxyethyl)benzamide (H_2L^1) and (*E*)-N-(2-(2-((2-hydroxynapthalen-1-yl)methylene) hydrazineyl)-2-oxyethyl)benzamide **(**H_2L^2)

TABLE-1
COLOUR, YIELD %, MELTING POINT, ANALYTICAL AND MOLAR CONDUCTANCE DATA OF THE Cu(II) COMPLEXES

Empirical formula; (m.w.), complex	Colour	Yield (%)	m.p. (ºC)	Elemental analysis (%): Found (calcd.)				Molar conductance (Ω^{-1} cm^2 mol^{-1})
				M	Cl	N	N_2H_4	
$[Cu(L^1)(H_2O)_2]H_2O$ (424.5), **1**	Pale green	80	>230	15.24 (14.9)	–	9.76 (9.89)	7.20 (7.53)	28.10
$[Cu(H_2L^2)(H_2O)Cl]$ $Cl{\cdot}H_2O$ (499.5), **2**	Olive green	80	270	12.71 (12.7)	14.84 (14.24)	8.31 (8.40)	6.97 (6.41)	84.50

acetate. Chlorine is present only in complex **2** and the molar conductance value [44] indicates the 1:1 electrolytic nature of the complex in 0.002 M DMSO at 25 ºC.

Thermal studies: The rate of heating was suitably controlled at 10º min^{-1} under nitrogen atmosphere and the weight loss was measured from 35-1000 ºC. The thermal data of complexes **1** and **2** is listed in Table-2.

The weight loss at different temperature ranges as shown by the thermograms (Fig. 1) indicates the presence of both lattice and coordinated water molecules in the copper(II) complexes. Complex **1** experiences a mass loss at 199-1005 ºC corresponding to one ligand molecule while a large weight loss for complex **2** corresponds to one ligand molecule and one chloride ion in one decomposition step. In all cases, the residues are carbon and metal oxides [45-48].

Infrared spectral studies: The IR spectral data of the ligands and complexes and the IR data obtained from the DFT studies are shown in Table-3 as parenthesis along with the respective spectral bands. The bonding sites of the ligands involved in complexation are studied by a careful comparison of the selected IR bands with those of the complexes.

In the IR spectrum of H_2L^1, the strong bands at 1699, 1531 and 1463 cm^{-1} are due to amide I, amide II and amide III modes of the hydrazidic moiety while the strong bands at 1622, 1500 and 1323 cm^{-1} are assigned to the amide bands of the benzamide group. The spectrum also exhibits strong bands at 1577 and 948 cm^{-1}, which may be assigned to ν(C=N) and ν(N-N) vibrations, respectively [49]. Similarly, the intense bands at 1697, 1551 and 1481 cm^{-1} and the bands at 1637, 1521 and 1411 cm^{-1} observed in the spectrum of H_2L^2 are assigned to the three amide bands of the hydrazide and benzamide moieties while the bands at 1575 and 989 cm^{-1} are due to ν(C=N) and ν(N-N) modes, respectively. In the spectra of copper(II) complexes, the amide bands of the benzamide moiety remained unaffected suggesting non-involvement of this group in complexation. However, in the spectrum of complex **1**, the amide bands of the hydrazidic group disappear and a sharp band diagnostic of >C=N-N=C< group appears at 1635 cm^{-1}. The appearance of this new band suggests the formation of a deprotonated complex in which H_2L^1 is coordinated in its enolic form. This can be explained by assuming the destruction

TABLE-2
DISSOCIATION STAGES CORRESPONDING TO WEIGHT LOSS OBSERVED IN TG CURVES AT DIFFERENT TEMPERATURE RANGES

Complexes	Dissociation stage	Temperature range in TG (ºC)	Weight loss (mg): Calcd. (obsd.)	Decomposition assignment
1	Stage 1	33-99	0.41 (0.46)	$-H_2O$
	Stage 2	99-199	0.40 (0.44)	$-2H_2O$
	Stage 3	199-1005	6.50 (5.79)	$-C_{17}H_{10}N_3O_2$
2	Stage 1	27-100	0.35 (0.20)	$-H_2O$
	Stage 2	100-200	0.34 (0.26)	$-H_2O$
	Stage 3	200-659	6.92 (6.35)	$-C_{20}H_{17}N_3O_3Cl$

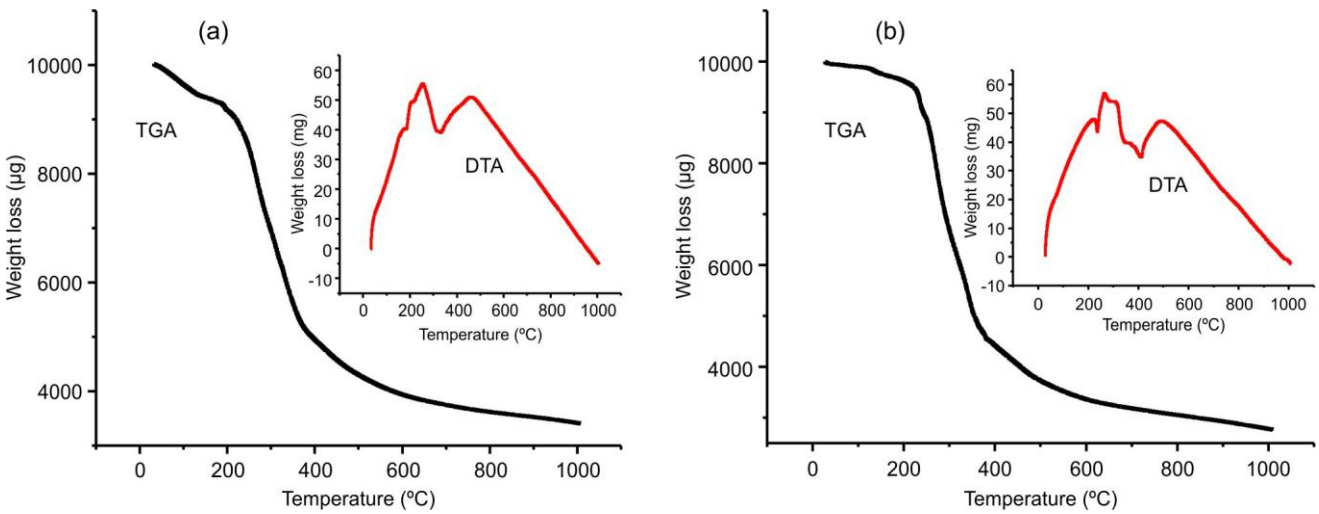

Fig. 1. TGA curves of (a) complex **1**; (b) complex **2** (Inset, DTA curves)

TABLE-3
SELECTED IR SPECTRAL BANDS (cm^{-1}) OF THE LIGANDS AND COMPLEXES AND THEIR ASSIGNMENTS

Compounds	Benzamide			Hydrazide			>C=N-N=C<	ν(M-N)	ν(M-O)
	Amide I	Amide II	Amide III	Amide I	Amide II	Amide III			
H_2L^1	1622	1500	1323	1699	1531	1463	–	–	–
H_2L^2	1637	1521	1411	1697	1551	1481	–	–	–
Complex **1**	1620 (1709)	1505 (1506)	1321 (1286)	–	–	–	1635 (1641)	550 (564)	452 (419)
Complex **2**	1635 (1702)	1521 (1601)	1420 (1452)	1620 (1644)	1511 (1512)	1419 (1512)	–	590 (550)	495 (432)

of hydrazidic carbonyl group through amide-imidol tautomerism and subsequent coordination of the imidol oxygen [50]. This is further supported by the appearance of a new peak characteristics of ν(NCO^-) in the 1598 cm^{-1} in the spectrum of complex **1** [51]. In case of complex **2**, the hydrazidic amide I and II bands show negative shift to 1620 cm^{-1} and 1511 cm^{-1}, respectively, showing the coordination of carbonyl oxygen in the amide form [49]. Involvement of azomethine nitrogen [50] in complexation is suggested by negative shift (40 cm^{-1}) of the ν(C=N) band and a positive shift (21 cm^{-1}, from 989 to 1010 cm^{-1}) in the ν(N-N) band in the spectrum of complex **2**, which is consistent from both experimental and theoretical results. The observed negative shift of the band due to the symmetric $(CO)_{phenolic}$ from 1255 cm^{-1} to 1215 cm^{-1} and disappearance of the $\nu(OH)_{phenol}$ band from the spectrum of complex **1** indicate the participation of phenolic oxygen in bonding. In the spectrum of complex **2**, the $\nu(OH)_{phenol}$ band is shifted from 1288 to 1249 cm^{-1} suggesting its involvement in complexation [49]. Furthermore, the appearance of broad bands at 3350 and 3344 cm^{-1} in the complexes may be assigned to ν(OH) of water molecules attached to the metal center. The coordination of the ligands with the metal ions was further confirmed by the appearance of new weak non-ligand bands in the 550-452 and 590-495 cm^{-1} in the IR spectra of the complexes assignable to ν(M-N) and ν(M-O) modes, respectively.

Electronic absorption spectra and magnetic moment studies: The electronic absorption spectra of the Schiff base ligands and its copper(II) complexes recorded in 0.002 M DMSO are shown in Fig. 2. The intense ligand bands in the 263-288 nm and weaker bands at 326-356 nm are due to π-π* transition of the aromatic rings and n-π* transition of imino group, respectively. In copper(II) complexes, these bands are shifted to longer wavelengths due to complexation with the metal ion. The intensity of the band due to the n-π* transition was observed to increase significantly in the spectra of Cu(II) complexes indicating that energy transfer occurs between the metal and the ligand and the 'n' electrons are involved in complex formation. The spectra of the complexes exhibit broad bands at 708 nm for copper **1** and 665 nm for copper **2**, which may be assigned to transitions $^2B_{1g} \rightarrow {}^2B_{2g}$ (D) for a distorted pentacoordinated geometry [51].

The magnetic moment values of the complexes **1** and **2**, 1.87 and 1.76 B.M., respectively, are normal for the presence of one unpaired electron suggesting the absence of any appreciable spin-spin coupling between unpaired electrons. However, they do not give any information regarding the stereochemistry of the complexes.

ESR studies: The solid-state ESR spectra of Cu(II) complexes **1** and **2** were recorded at liquid nitrogen temperature (LNT), as shown in Fig. 3. The spectra exhibit anisotropic features, characteristic of Cu(II) complexes. The $g_{\parallel}$ and $g_{\perp}$ values obtained are, respectively, 2.220 and 2.011 for complex **1** and 2.102 and 2.017 for complex **2**. The g-values are lesser than 2.3 indicating the covalent character of the M-L bond. The trend in g-values for both complexes, $g_{\parallel} > g_{\perp} > g_e$ (2.0023), suggests tetragonal elongation along *z*-axis and the presence

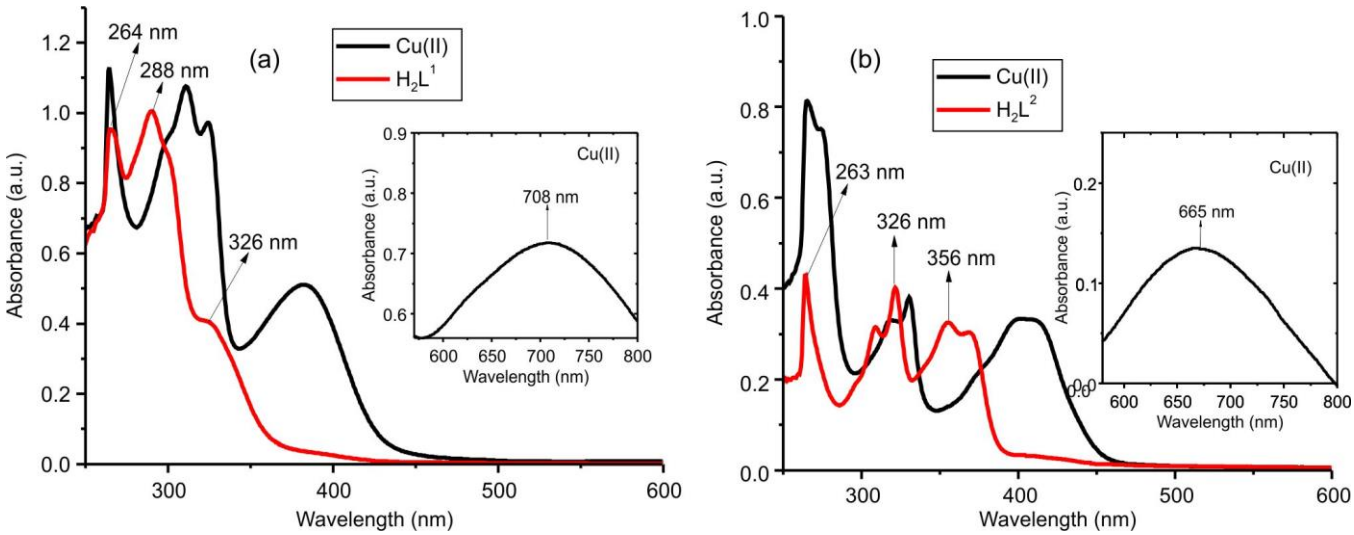

Fig. 2. Electronic absorption spectra of (a) complex **1** and (b) complex **2** (Inset, *d-d* transitions of the complexes)

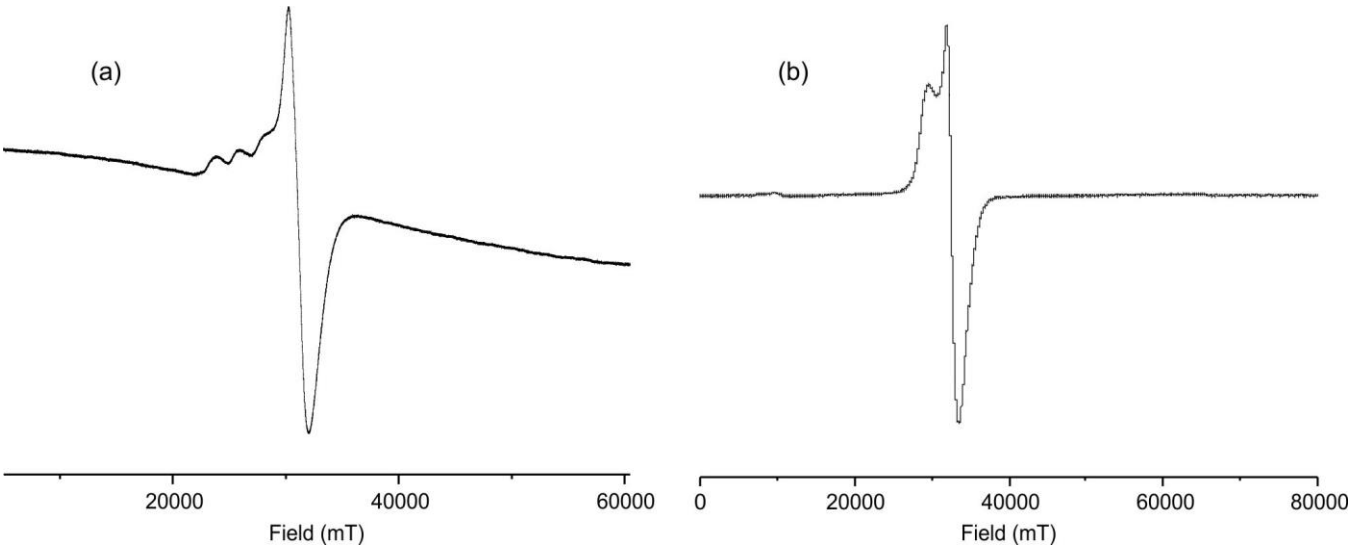

Fig. 3. Solid ESR spectra of the complexes at LNT, (a) complex **1**, (b) complex **2**

of the unpaired electron in b_{1g} ($d_{x^2-y^2}$) orbital [52-54]. Hyperfine coupling constant, $A_{\parallel}$, 150 G, obtained from the spectrum of complex **1** suggests small axial interaction. The bonding parameters *viz*. α^2 (covalency of in-plane σ bonds), β^2 (in-plane π bonds), γ^2 (out-plane π bonds) and the orbital reduction factor ($K_{\parallel}$ and $K_{\perp}$) were evaluated using the *d-d* transition energy of **1** (708 nm) and the spin orbit coupling constant for the free Cu(II) ion (λ_o = 828 cm^{-1}) from the expressions 1-5 [54,55].

$$\alpha^2 = -\left(\frac{A_{\parallel}}{0.036}\right) + (g_{\parallel} - 2.002) + \frac{3}{7}(g_{\perp} - 2.002) + 0.04 \quad (1)$$

$$K_{\parallel}^2 = (g_{\parallel} - 2.0023)\frac{E_{d-d}}{8\lambda_o} \quad (2)$$

$$K_{\perp}^2 = (g_{\perp} - 2.0023)\frac{E_{d-d}}{2\lambda_o} \quad (3)$$

$$K_{\parallel} = \alpha^2\beta^2 \quad (4)$$

$$K_{\perp} = \alpha^2\gamma^2 \quad (5)$$

The value of α^2 (0.64) shows high covalent character of the Cu-L bond in the complex **1**. The values of β^2 (0.237) and γ^2 (0.089) indicate that there is interaction in the in-plane and out-of-plane π-bonding between Cu(II) ion and the ligand. The higher value of $K_{\parallel}$ (0.152) compared to $K_{\perp}$ (0.057) indicates a greater contribution from out-of-plane π-bonding than in-plane π-bonding in the M-L bonding. These observations reveal a lower symmetry structure and thus support square pyramidal geometry for complex **1**. The geometric parameter, $G = \frac{g_{\parallel} - 2}{g_{\perp} - 2}$ measures the exchange interaction between the metal centers in a polycrystalline solid. G > 4 for complexes of weak field ligands with negligible exchange interaction and G < 4 for complexes having strong field ligands with a considerable exchange interaction [56]. The G-values, 5.42 for complex **1** and 6.00 for complex **2** indicate that the ligands are weak field ligands and there is negligible exchange interaction between the Cu-Cu centers in the complexes [57]. In absence of the single crystal data, no concrete structure could be ascertained. Both ESR and DFT studies indicate that the complexes **1** and **2** are penta-coordinated. However, though ESR studies suggest tetragonally elongated square pyramidal structure with the unpaired electron in the b_{1g} ($d_{x^2-y^2}$) orbital for both complexes, the optimized structure obtained from DFT studies for complex **2** is trigonal bipyramidal. It has been reported that most commonly five coordinated complexes have geometries intermediate between the two limiting geometries perhaps because of the small energy barrier between the square pyramidal and trigonal bipyramidal structures [58,59]. Thus, it may be assumed that square pyramidal structure is the preferred structure for complex **2** in the solid state at LNT while it might have adopted the tetragonally compressed one at room temperature.

Mass spectral studies: The ESI-mass spectra of complexes **1** and **2** are given in Fig. 4. The mass spectrum of complex **1** shows the molecular ion peak at *m/z* 442.5 corresponding to composition $[Cu(L^1)(H_2O)_2]H_2O$ proposed based on elemental and TGA data and the peaks at *m/z* 424.5 is due to the molecular mass after losing one molecule of water. The peak at *m/z* 847.6 corresponds to other species having an M:L ratio which is not supported by the elemental analysis data. The mass spectrum of complex **2** shows a molecular ion peak at *m/z* 499.5 corresponding to the composition $[Cu(H_2L^2)(H_2O)Cl]Cl$. Appearance of the peaks at *m/z* > molecular mass number suggests rearrangement of the fragments or collision of the molecular ions with neutral atoms or molecules.

Powder XRD studies: The powder X-ray diffraction pattern of Cu(II) complexes **1** and **2** were examined at the wavelength 1.5406 Å operating at a voltage of 40 kV and a current of 20 mA and the diffraction lines of the complexes could be successfully indexed [60]. Both the Schiff base copper(II) complexes are crystalline in nature. The crystallinity index for complexes **1** and **2** are 0.703 and 1.052, respectively.

Antidiabetic activities: The antidiabetic activities of the Schiff base ligands and its Cu(II) complexes were screened *in vitro* by using α-glucosidase enzyme activity inhibition

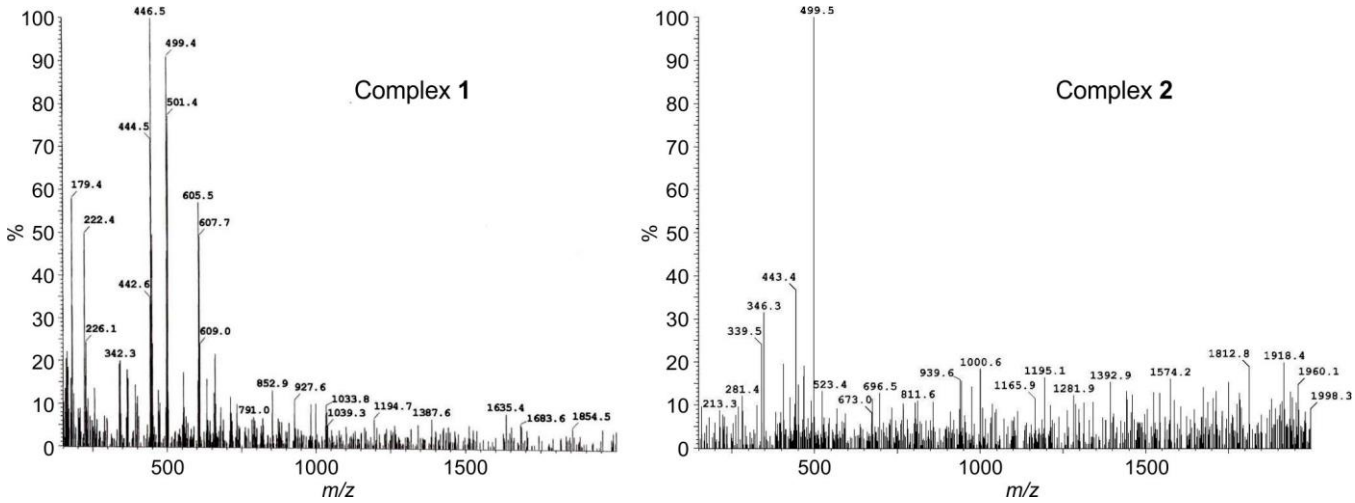

Fig. 4. Mass spectrum of complex **1** and complex **2**

assay as compared to the standard drug, acarbose. The α-glucosidase inhibition assay revealed that the ligands exhibited negligible antidiabetic activity across all solvent-based test samples, showing significantly lower inhibition values compared to the standard drug, acarbose. However, the both Cu(II) complexes have shown significant effect in antidiabetic test *i.e.* they have shown significant enzyme inhibition activity in the range of 94.9% to 98.3%, which are significantly higher than that of the standard drug acarbose which shows only 61.71% α-glucosidase enzyme inhibition activity. The 50% enzyme inhibition concentration (IC_{50}) of the Schiff base ligands and its Cu(II) complexes in various solvents as compared to the standard drug, acarbose are shown in Fig. 5. Among the samples in different solvents, ethyl acetate shows the lowest value (4.30 ± 0.29 µg/mL) of IC_{50} followed by DMSO (5.84 ± 1.35 µg/mL) as compared to acarbose (8.64 ± 2.68 µg/mL) indicating that these two samples possess significant antidiabetic activities [61]. The other solvents like MeOH, DMSO, water, $CHCl_3$, acarbose in water (ACBW) and EtOH (E) have shown higher values of IC_{50} than acarbose, which reveals insignificant antidiabetic properties of these samples. Moreover, the hill co-efficient values (ηH) of solvents *e.g.* MeOH, water, $CHCl_3$, DMSO and ethyl acetate are more than 1 (ηH > 1) (Table-4), demonstrating the positive cooperative binding of the complexes to the active sites of enzyme, which subsequently results in the suppression of the enzyme's activity [61-64]. Based on the antidiabetic activity assay of the Schiff base ligands and its Cu(II) complexes, it is suggested that the compounds in solvents ethyl acetate and G may be subjected to further pre-clinical studies on their antidiabetic properties, absorption, dissorption, metabolisms and excretion (ADME) properties and toxicity evaluation through *in vivo* bioassays. This could lead to evaluation of the compounds as potential drug molecules for treatment and management of diabetes.

Computational DFT studies: Complex **1** is neutral as the doubly deprotonated ligand undergoes complexation with the Cu^{2+} ion while the complex **2** has a +1 charge as it consists of a neutral ligand and one negatively charge chloride ion and the charge on **2** is balanced by the chloride ions present outside the coordination sphere of the complex. During the calculation,

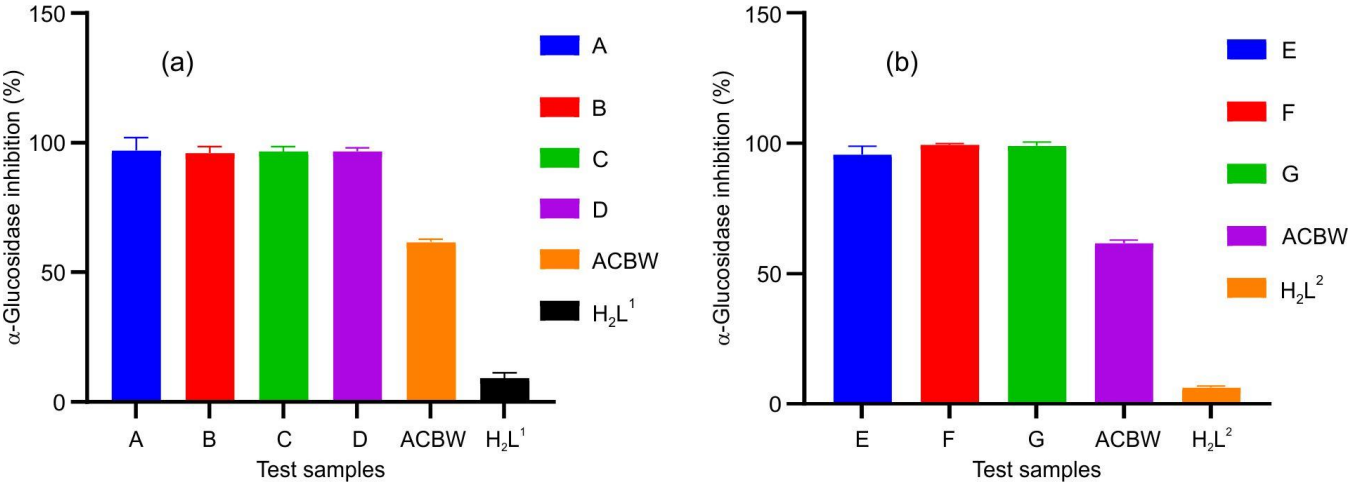

Fig. 5. α-Glucosidase inhibition properties (%) of the ligands, complexes and acarbose in different solvents, T-bars on the histogram represent standard deviation (SD) of the mean values. (a) Complex **1** in MeOH (A), DMSO (B), water (C), $CHCl_3$ (D), acarbose in water (ACBW) and H_2L^1 (in any of the above solvents) (b) Complex **2** in EtOH (E), ethyl acetate (F), DMSO (G), acarbose in water (ACBW) and H_2L^2 (in any of the above solvents)

TABLE-4
IC_{50} AND HILL COEFFICIENT (ηH) VALUES
OF α-GLUCOSIDASE INHIBITION PROPERTIES
OF Cu(II) COMPLEXES AND STANDARD
COMPOUNDS IN DIFFERENT SOLVENTS

Samples	IC_{50} (μg/mL)	SD (±)	Hill coefficient (ηH)
MeOH	9.97	2.86	6.06
DMSO (H_2L^1)	12.09	2.09	0.60
Water	9.43	1.42	26.96
$CHCl_3$	12.86	3.28	5.53
EtOH	12.16	0.88	0.26
Ethyl acetate	4.30	0.29	8.67
DMSO (H_2L^2)	5.84	1.35	1.01
ACBW	8.64	2.68	6.14

the multiplicities for both Cu(II) complexes were taken as a doublet as the metal ion has d^9 configuration. Complex **1** has a square pyramidal structure due to the complexation of the tridentate ligand with two water molecules whereas complex **2** has a trigonal bipyramidal structure where the complexation involves bonding with one tridentate ligand molecule, one chlorine atom and a water molecule. The optimized geometries of the complexes **1** and **2** are shown in Fig. 6 and the computed optimized results of bond distances, bond angles, bond order and Mulliken atomic charges are summarized in Tables 5 and 6. The designations of the atoms in both the complexes are done in such a way that the metal centre is given **1** and the ligand donor atoms directly attached to the metal are numbered from **2-6**.

For complex **1**, the bond distances of the equatorial plane are in the range of 1.89-2.04 Å, whereas that of axial Cu–O bond is 2.46 Å. The nitrogen atom designated as **3** has the minimum Mulliken atomic charge of -0.31 and it is responsible for having the highest bond order of 1 between the bond 1-3. The square bipyramidal geometry obtained in the optimization is not perfect as it involves some distortions. The equatorial angles that should have been perpendicular were distorted by a maximum of ± 8.8º while the axial angles were distorted by ± 10.4º. However, the linear angles ∠ 214 and ∠ 315 were distorted by a maximum of ± 7º from the normal 180º. For complex **2**, the coordinating N of the ligand, designated as 5, has minimum electron charge density and hence the lone pair

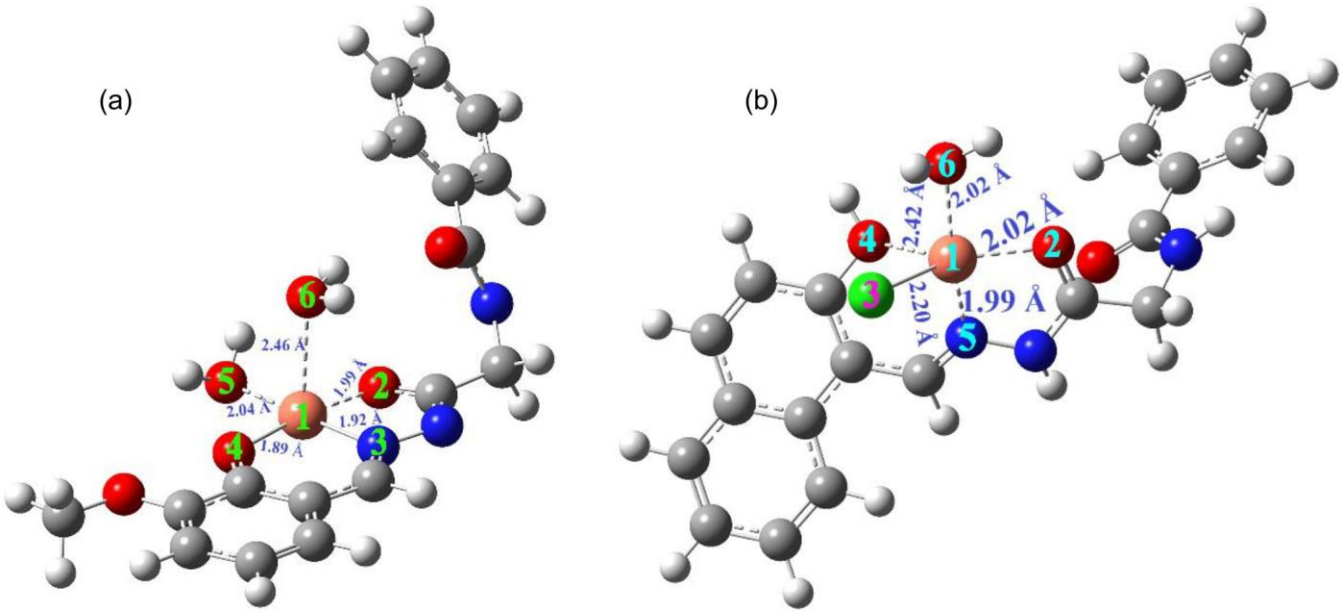

Fig. 6. Optimized structures of (a) complex **1** having square pyramidal geometry, (b) complex **2** having trigonal bipyramidal geometry

TABLE-5
Cu(II) COMPLEX **1** SHOWING BOND DISTANCES, BOND ORDER, BOND ANGLES,
MULLIKEN ATOMIC CHARGES AROUND THE SQUARE PYRAMIDAL GEOMETRICAL CENTRE

Bond distance (Å)		Bond order		Bond angles (º)		Mulliken atomic charges	
Bond		Bond		Angles		Atoms	
1-2	1.99	1-2	0.5	∠ 213	81.2	1	0.08
1-3	1.92	1-3	1.0	∠ 314	94.9	2	-0.65
1-4	1.89	1-4	0.5	∠ 415	87.9	3	-0.31
1-5	2.04	1-5	0.5	∠ 512	95.8	4	-0.51
1-6	2.46	1-6	0.5	∠ 612	85.8	5	-0.51
				∠ 613	94.1	6	-0.57
				∠ 614	100.4		
				∠ 615	87.1		
				∠ 214	173.0		
				∠ 315	176.7		

TABLE-6
Cu(II) COMPLEX **2** SHOWING BOND DISTANCES, BOND ORDER, BOND ANGLES, MULLIKEN ATOMIC CHARGES AROUND THE TRIGINAL BIPYRAMIDAL GEOMETRICAL CENTRE

Bond distance (Å)		Bond order		Bond angles (º)		Mulliken atomic charges	
Bond		Bond		Angles		Atoms	
1-2	2.02	1-2	0.5	∠ 213	149.7	1	0.07
1-3	2.20	1-3	0.5	∠ 314	90.1	2	-0.48
1-4	2.42	1-4	0.5	∠ 412	119.5	3	-0.24
1-5	1.99	1-5	0.5	∠ 512	80.1	4	-0.60
1-6	2.02	1-6	0.5	∠ 513	103.5	5	-0.12
				∠ 514	75.3	6	-0.42
				∠ 612	92.5		
				∠ 613	90.3		
				∠ 614	96.1		
				∠ 516	163.6		

electron present on it was readily donated during coordination resulting in the formation of shortest bond distance (1-5) of 1.99 Å. Besides, the distortion shown by complex **2** is larger with equatorial distortion of up to ± 29.9º, axial distortion of up to ± 14.7º and linear axial axis distorted by 16.4º.

The electron donor capability of a molecule is reflected in its highest occupied molecular orbital (HOMO), whereas the electron acceptor ability is represented by the lowest unoccupied molecular orbital (LUMO). The molecular orbitals with the energy gap is shown in Fig. 7 and the two colours, green and brown, respectively indicate the positive and negative phases of the wavefunction representing the molecular orbitals. Molecules characterized by large HOMO-LUMO energy gaps tend to exhibit stability and reduced chemical reactivity. Conversely, molecules with narrow energy gaps demonstrate enhanced conductivity, heightened chemical reactivity and diminished kinetic stability [65]. The HOMO-LUMO energy levels of the complexes were calculated using TD-DFT at the following level of theory, M06/6-31+G(d,p) for O, N and M06/def2-SVP for H, C and Cu. The HOMO-LUMO gap obtained from the results of geometry optimization underestimated the optical excitation gap whereas the optical gap from TD-DFT calculations considers many-body interactions and yields results closer to experimental absorption energy. The value of the energy gap between HOMO–LUMO for complex **1** is 1.23 eV and that of complex **2** is 0.74 eV. The observed HOMO–LUMO gap indicates that **1** is more stable than **2**.

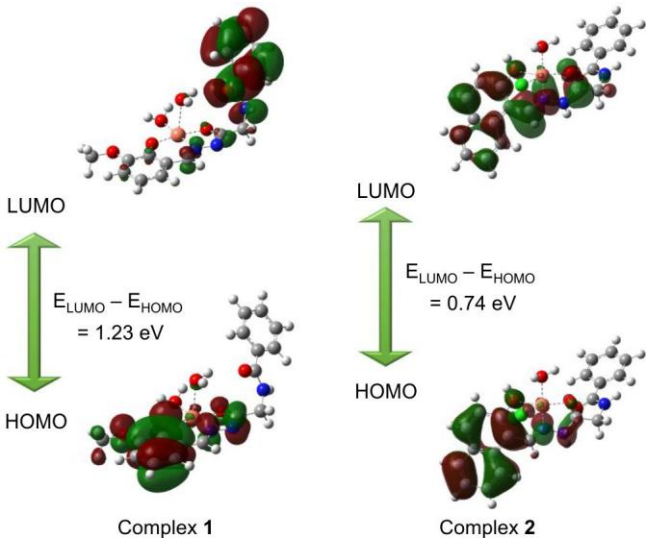

Fig. 7. Molecular orbitals with HOMO-LUMO energy gap for the Cu(II) complexes

The comparison of Mulliken, Hirshfeld and Charge Model 5 (CM5) charges for the complexes **1** and **2** has been made through DFT studies and the result is shown in Fig. 8. The charges and corresponding molecular dipole moments predicted through CM5 lead to more accurate dipole moments as compared to the original Hirshfeld charges, Mulliken charges, or any other models [35]. In both complexes, it has been observed that, particularly at the metal center, the charge predicted by the CM5 model gives the highest value followed by the Hirshfeld and Mulliken charges, respectively. Mulliken and Hirshfeld underpredicted and overpredicted Cu charge respectively due to basis set effects and density-based nature, however, CM5 would give a more reliable Cu charge, matching with the experimental results. Thus, CM5 yields a better charge predicting these Cu(II) complexes [35,66].

Electronic spin density is positive in areas where an electron is more likely to be found in the α spin state and negative where an electron is more likely to be found in the β spin state and the electron spin densities of the complexes are given in Fig. 9. Negative spin density is shown in the green lobe whereas the positive spin density is in blue. In complex **1**, the electrons exist in the α spin state for the ligands in the square base, except the water molecule at the peak position with no spin density, however, the central metal Cu has β spin state. Similarly for complex **2**, the central atom has β spin state and ligands have α spin state except for the phenolic ligand with no spin density. The green and blue lobes illustrate areas of unpaired electron density, primarily concentrated around the central Cu atom and its nearby ligands. It is observed that while the unpaired electron is mainly centered on Cu, some delocalization onto the ligands also occurs.

Conclusion

Two new Schiff bases, (*E*)-N-(2-(2-(2-hydroxy-3-methoxybenzylidene)hydrazineyl)-2-oxyethyl)benzylidene)hydrazineyl)-2-oxyethyl)benzamide (H_2L^1), (*E*)-N-(2-((2-hydroxynapthalen-1-yl)methylene)hydrazineyl)-2-oxyethyl)benzamide (H_2L^2) react with $CuCl_2$ to form stable Cu(II) pentacoordinated comp-

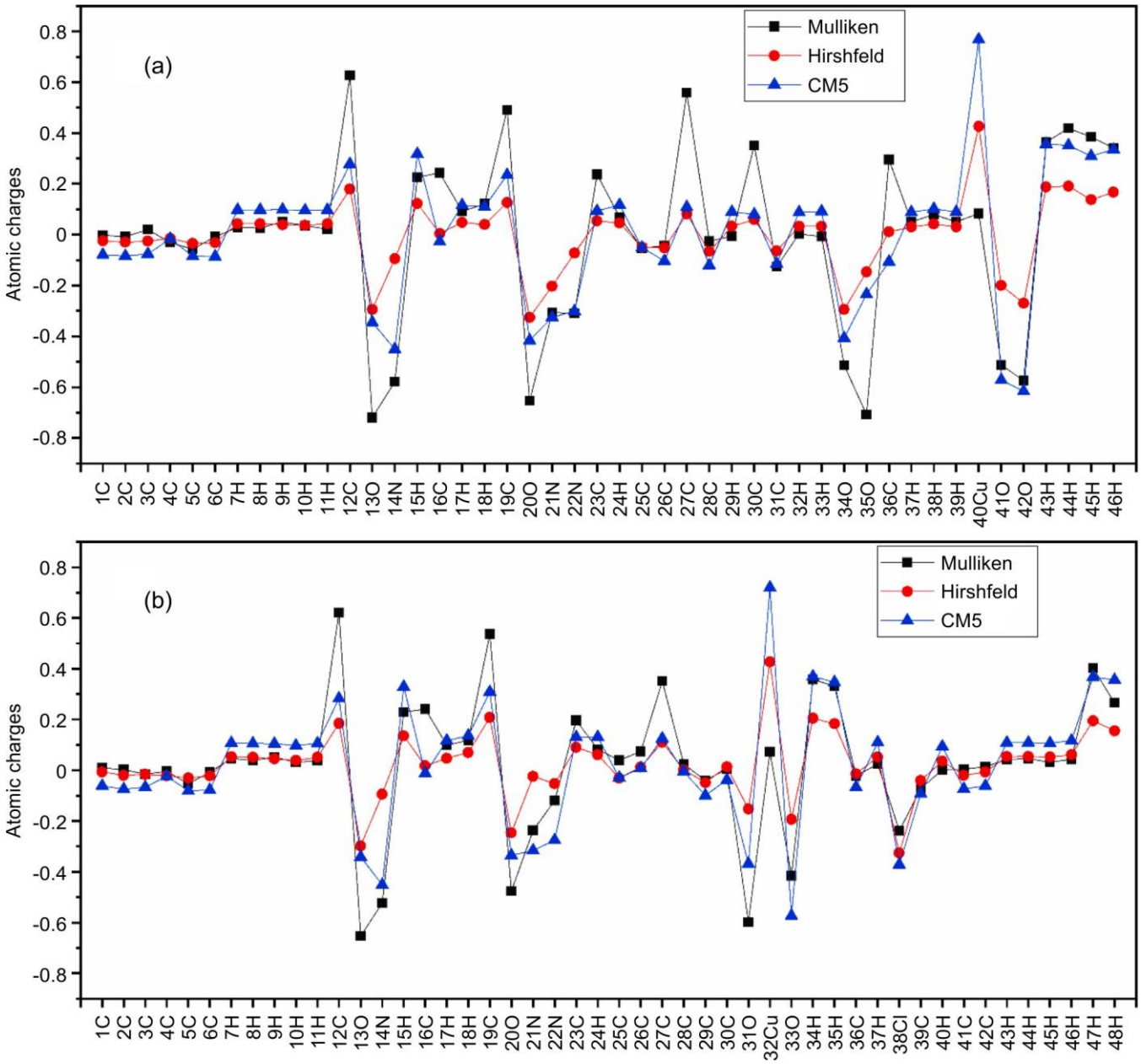

Fig. 8. Comparison of Mulliken, Hirshfeld and CM5 Charges for (a) complex **1** and (b) complex **2**

lexes having the molecular formula $[Cu(L^1)(H_2O)_2]\cdot H_2O$ and $[Cu(H_2L^2)(H_2O)Cl]Cl\cdot H_2O$. Elemental and thermal analyses confirm the presence of water molecules in the complexes. ESR studies of the Cu(II) complexes suggest the tetragonal elongation for both complexes though DFT studies indicate the optimized geometry for complex **2** as trigonal bipyramid. The IR spectral analysis and the optimized structures of the complexes obtained from DFT studies show that H_2L^1 binds to Cu(II) ion in complex **1** as a dinegative tridentate species bonding through the carbonyl-O, azomethine-N and phenolate-O while in complex **2**, H_2L^2 acts as a neutral tridentate species using carbonyl-O, azomethine-N and phenolic-O of the aldehydic group as bonding sites. The α-glucosidase enzyme assay indicates that the ligands have no significant antidiabetic properties while the both Cu(II) complexes exhibit significantly high enzyme inhibition activity in the range of 94.9% to 98.3% much higher than the activity of the standard drug acarbose, which shows only 61.71% α-glucosidase enzyme inhibition activity. The significant inhibition activities indicate the potential of the copper(II) complexes with N,O-donor Schiff base ligands for the practical applications, which merits further investigation.

ACKNOWLEDGEMENTS

The authors acknowledge Manipur University for its financial support in the form of University fellowship to Sapam Saya Devi, SAIF, Central Drug Research Institute, Lucknow for mass spectra, ^{1}H NMR and CHN analysis of the ligand and the complexes, IIT Roorkee for TG-DT analysis and DST, New Delhi (research project EEQ/2016/000597) for DFT studies.

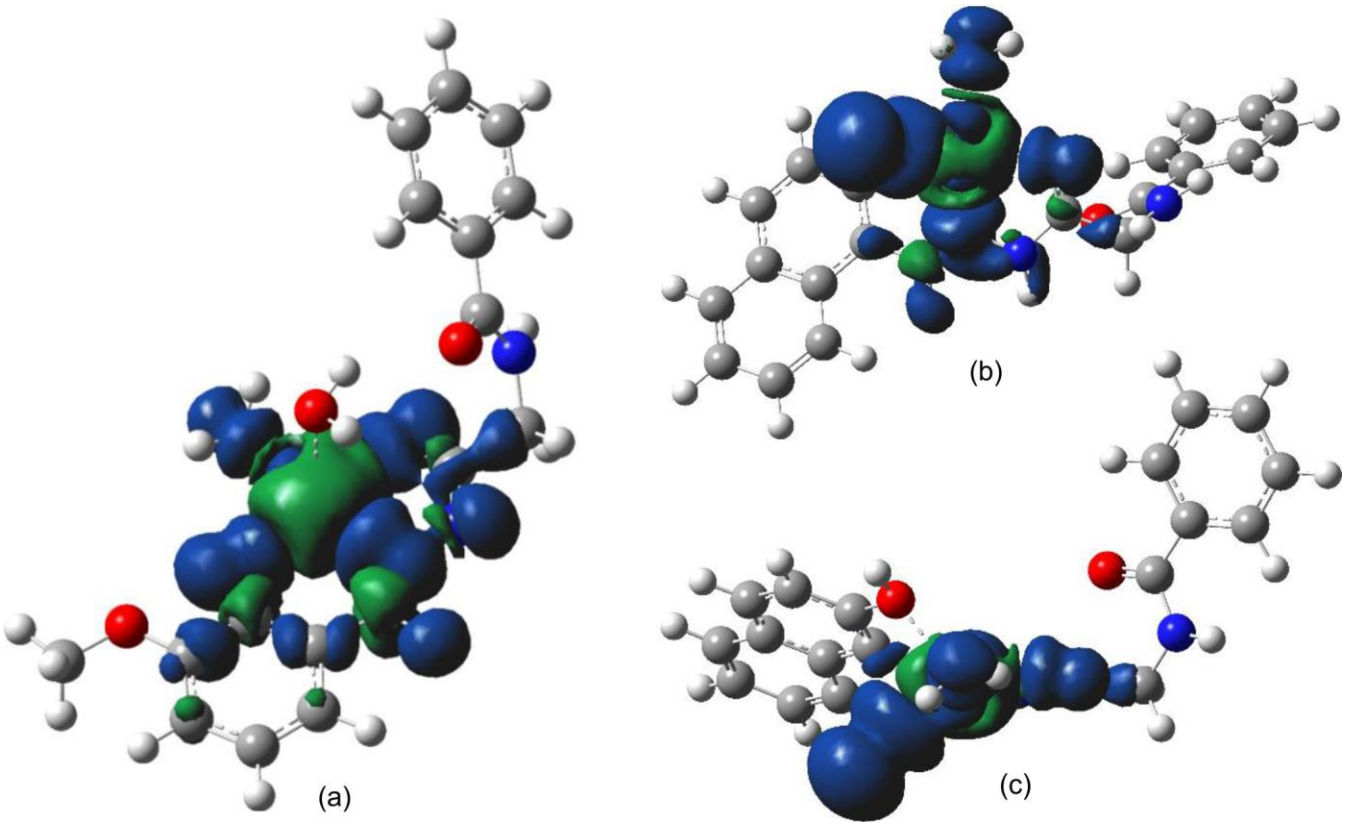

Fig. 9. Electron spin density figures (isovalue 0.0004) for (a) complex **1** and (b) complex **2** (side view), (c) complex **2** (top view)

CONFLICT OF INTEREST

The authors declare that there is no conflict of interests regarding the publication of this article.

REFERENCES

1. E. Raczuk, B. Dmochowska, J. Samaszko-Fiertek and J. Madaj, *Molecules*, **27**, 787 (2022); https://doi.org/10.3390/molecules27030787
2. A.I.A. Soliman, M. Sayed, M.M. Elshanawany, O. Younis, M. Ahmed, A.M. Kamal El-Dean, A.-M.A. Abdel-Wahab, J. Wachtveitl, M. Braun, P. Fatehi and M.S. Tolba, *ACS Omega*, **7**, 10178 (2022); https://doi.org/10.1021/acsomega.1c06636
3. M. Arifuzzaman, M.R. Karim, T.A. Siddiquee, A.H. Mirza and M.A. Ali, *Int. J. Org. Chem.*, **03**, 81 (2013); https://doi.org/10.4236/ijoc.2013.31009
4. E. Sinn and C.M. Harris, *Coord. Chem. Rev.*, **4**, 391 (1969); https://doi.org/10.1016/S0010-8545(00)80080-6
5. P.B. Sreeja, M.R. Prathapachandra Kurup, A. Kishore and C. Jasmin, *Polyhedron*, **23**, 575 (2004); https://doi.org/10.1016/j.poly.2003.11.005
6. P.B. Sreeja and M.R.P. Kurup, *Spectrochim. Acta A Mol. Biomol. Spectrosc.*, **61**, 331 (2005); https://doi.org/10.1016/j.saa.2004.04.001
7. D. Kovala-Demertzi, A. Domopoulou, M.A. Demertzis, G. Valle and A. Papageorgiou, *J. Inorg. Biochem.*, **68**, 147 (1997); https://doi.org/10.1016/S0162-0134(97)00087-1
8. D. Kovala-Demertzi, M.A. Demertzis, V. Varagi, A. Papageorgiou, D. Mourelatos, E. Mioglou, Z. Iakovidou and A. Kotsis, *Chemotherapy*, **44**, 421 (1998); https://doi.org/10.1159/000007154
9. M. Tümer, H. Köksal, M.K. Sener and S. Serin, *Transition Met. Chem.*, **24**, 414 (1999); https://doi.org/10.1023/A:1006973823926
10. N. Raman, J. Dhaveethu Raja and A. Sakthivel, *J. Chem. Sci.*, **119**, 303 (2007); https://doi.org/10.1007/s12039-007-0041-5
11. E.W. Ainscough, A.M. Brodie, A.J. Dobbs, J.D. Ranford and J.M. Waters, *Inorg. Chim. Acta*, **267**, 27 (1998); https://doi.org/10.1016/S0020-1693(97)05548-5
12. B. Koçyigit Kaymakçioglu and S. Rollas, *Farmaco*, **57**, 595 (2002); https://doi.org/10.1016/S0014-827X(02)01255-7
13. S.N. Pandeya, D. Sriram, G. Nath and E. De Clercq, *Farmaco*, **54**, 624 (1999); https://doi.org/10.1016/S0014-827X(99)00075-0
14. E.M. Hodnett and W.J. Dunn, *J. Med. Chem.*, **13**, 768 (1970); https://doi.org/10.1021/jm00298a054
15. J. Vanèo, J. Marek, Z. Trávníèek, E. Raèanská, J. Muselík and O. Švajlenová, *J. Inorg. Biochem.*, **102**, 595 (2008); https://doi.org/10.1016/j.jinorgbio.2007.10.003
16. A. Hameed, M. Al-Rashida, M. Uroos, S. Abid Ali and K.M. Khan, *Expert Opin. Ther. Pat.*, **27**, 63 (2017); https://doi.org/10.1080/13543776.2017.1252752
17. C.M. Sharaby, *Spectrochim. Acta A Mol. Biomol. Spectrosc.*, **66**, 1271 (2007); https://doi.org/10.1016/j.saa.2006.05.030
18. M. Hosseini, Z. Vaezi, M.R. Ganjali, F. Faridbod, S.D. Abkenar, K. Alizadeh and M. Salavati-Niasari, *Spectrochim. Acta A Mol. Biomol. Spectrosc.*, **75**, 978 (2010); https://doi.org/10.1016/j.saa.2009.12.016
19. X. Zhong, Z. Li, R. Shi, L. Yan, Y. Zhu and H. Li, *ACS Appl. Nano Mater.*, **5**, 13998 (2022); https://doi.org/10.1021/acsanm.2c03477
20. J. Costamagna, J. Vargas, R. Latorre, A. Alvarado and G. Mena, *Coord. Chem. Rev.*, **119**, 67 (1992); https://doi.org/10.1016/0010-8545(92)80030-U
21. P.G. Cozzi, *Chem. Soc. Rev.*, **33**, 410 (2004); https://doi.org/10.1039/B307853C
22. L.H. Uppadine, J.-P. Gisselbrecht and J.-M. Lehn, *Chem. Commun.*, **718–719**, 718 (2004); https://doi.org/10.1039/B315352E

23. A. Wood, W. Aris and D.J.R. Brook, *Inorg. Chem.*, **43**, 8355 (2004); https://doi.org/10.1021/ic0492688
24. M.R. Bermejo, R. Pedrido, A.M. González-Noya, M.J. Romero, M. Vázquez and L. Sorace, *New J. Chem.*, **27**, 1753 (2003); https://doi.org/10.1039/B305354G
25. S. Naskar, M. Corbella, A.J. Blake and S.K. Chattopadhyay, *Dalton Trans.*, 1150 (2007); https://doi.org/10.1039/b615004g
26. R. Ganguly, B. Sreenivasulu and J.J. Vittal, *Coord. Chem. Rev.*, **252**, 1027 (2008); https://doi.org/10.1016/j.ccr.2008.01.005
27. M.J. O'Donnell, *Tetrahedron*, **75**, 3667 (2019); https://doi.org/10.1016/j.tet.2019.03.029
28. A. Anagnostopoulos and S. Hadjispyrou, *J. Inorg. Biochem.*, **57**, 279 (1995); https://doi.org/10.1016/0162-0134(94)00033-7
29. P.D. Thangjam and L. Rajkumari, *J. Chem. Eng. Data*, **55**, 1166 (2010); https://doi.org/10.1021/je900583g
30. T. Devi and R. Lonibala, *Asian J. Chem.*, **22**, 5369 (2010).
31. T. Devi and R. Lonibala, *Orient. J. Chem.*, **30**, 2029 (2014); https://doi.org/10.13005/ojc/300468
32. R.K. Lonibala, T.R. Rao and R.K.B. Devi, *J. Chem. Sci.*, **118**, 327 (2006); https://doi.org/10.1007/BF02708526
33. A. Bhunia, S. Manna, S. Mistri, A. Paul, R.K. Manne, M.K. Santra, V. Bertolasi and S. Chandra Manna, *RSC Adv.*, **5**, 67727 (2015); https://doi.org/10.1039/C5RA12324K
34. K. Nejati, A. Bakhtiari, R. Bikas and J. Rahimpour, *J. Mol. Struct.*, **1192**, 217 (2019); https://doi.org/10.1016/j.molstruc.2019.04.135
35. A.V. Marenich, S.V. Jerome, C.J. Cramer and D.G. Truhlar, *J. Chem. Theory Comput.*, **8**, 527 (2012); https://doi.org/10.1021/ct200866d
36. A.I. Vogel, A Text Book of Quantitative Inorganic Analysis, London: ELBS & Longsman, pp. 358-460 (1961).
37. D. Kumar, H. Kumar, J.R. Vedasiromoni and B.C. Pal, *Phytochem. Anal.*, **23**, 421 (2012); https://doi.org/10.1002/pca.1375
38. B.G. Janesko, K.B. Wiberg, G. Scalmani and M.J. Frisch, *J. Chem. Theory Comput.*, **12**, 3185 (2016); https://doi.org/10.1021/acs.jctc.6b00343
39. Y. Zhao and D.G. Truhlar, *Theor. Chem. Acc.*, **120**, 215 (2008); https://doi.org/10.1007/s00214-007-0310-x
40. R. Ditchfield, W.J. Hehre and J.A. Pople, *J. Chem. Phys.*, **54**, 724 (1971); https://doi.org/10.1063/1.1674902
41. F. Weigend, *Phys. Chem. Chem. Phys.*, **8**, 1057 (2006); https://doi.org/10.1039/b515623h
42. F. Weigend and R. Ahlrichs, *Phys. Chem. Chem. Phys.*, **7**, 3297 (2005); https://doi.org/10.1039/b508541a
43. T.R. Rao, M. Sahay and R.C. Aggarwal, *Synth. React. Inorg. Met.-Org. Chem.*, **15**, 209 (1985); https://doi.org/10.1080/00945718508059381
44. W.J. Geary, *Coord. Chem. Rev.*, **7**, 81 (1971); https://doi.org/10.1016/S0010-8545(00)80009-0
45. M.L. Dianu, A. Kriza and A.M. Musuc, *J. Therm. Anal. Calorim.*, **112**, 585 (2013); https://doi.org/10.1007/s10973-012-2578-x
46. G. Bannach, A.B. Siqueira, E.Y. Ionashiro, E.C. Rodrigues and M. Ionashiro, *J. Therm. Anal. Calorim.*, **90**, 873 (2007); https://doi.org/10.1007/s10973-005-7060-6
47. W. Ferenc and A. Walków-Dziewulska, *J. Therm. Anal. Calorim.*, **63**, 865 (2001); https://doi.org/10.1023/A:1010120911658
48. L.V. Ababei, A. Kriza, A.M. Musuc, C. Andronescu and E.A. Rogozea, *J. Therm. Anal. Calorim.*, **101**, 987 (2010); https://doi.org/10.1007/s10973-009-0560-z
49. K. Nakamoto, Infrared and Raman Spectra of Inorganic and Coordination Compounds, Wiley: New York, edn. 4 (1986).
50. A. Braibanti, F. Dallavalle, M.A. Pellinghelli and E. Leporati, *Inorg. Chem.*, **7**, 1430 (1968); https://doi.org/10.1021/ic50065a034
51. A.B.P. Lever and H.B. Gray, *Acc. Chem. Res.*, **11**, 348 (1978); https://doi.org/10.1021/ar50129a005
52. K.B. Gudasi, S.A. Patil, R.S. Vadavi, R.V. Shenoy and M.S. Patil, *J. Serb. Chem. Soc.*, **71**, 529 (2006); https://doi.org/10.2298/JSC0605529G
53. D.E. Billing and B.J. Hathaway, *J. Chem. Phys.*, **50**, 1476 (1969); https://doi.org/10.1063/1.1671216
54. B.J. Hathaway and P.G. Hodgson, *J. Inorg. Nucl. Chem.*, **35**, 4071 (1973); https://doi.org/10.1016/0022-1902(73)80395-1
55. R.C. Van Landschoot, J.A.M. Van Hest and J. Reedijk, *J. Inorg. Nucl. Chem.*, **38**, 185 (1976); https://doi.org/10.1016/0022-1902(76)80081-4
56. B.A. Goodman and J.B. Raynor, *Adv. Inorg. Chem.*, **13**, 135 (1970); https://doi.org/10.1016/S0065-2792(08)60336-2
57. D.X. West, *J. Inorg. Nucl. Chem.*, **43**, 3169 (1981); https://doi.org/10.1016/0022-1902(81)80082-6
58. A. Bencini, I. Bertini, D. Gatteschi and A. Scozzafava, *Inorg. Chem.*, **17**, 3194 (1978); https://doi.org/10.1021/ic50189a047
59. J.A. Howard, R. Sutcliffe, J.S. Tse and B. Mile, *Chem. Phys. Lett.*, **94**, 561 (1983); https://doi.org/10.1016/0009-2614(83)85056-8
60. L.V. Azaroff and M.J. Bueger, The Powder Method in X-Ray Crystallography, New York: McGraw Hill (1958).
61. P. Debnath, P. Debnath, Th.S. Devi, S.S.K. Singh, A. Bhattacharya, K.S. Singh, M. Roy and T.K. Misra, *J. Coord. Chem.*, **75**, 3015 (2022); https://doi.org/10.1080/00958972.2022.2155145
62. P. Debnath, K.S. Singh, K.K. Singh, S. Sureshkumar Singh, L. Sieroñ and W. Maniukiewicz, *New J. Chem.*, **44**, 5862 (2020); https://doi.org/10.1039/D0NJ00536C
63. M. Roy, S. Roy, K.S. Singh, J. Kalita and S.S. Singh, *New J. Chem.*, **40**, 1471 (2016); https://doi.org/10.1039/C5NJ02637G
64. M. Roy, S. Roy, K.S. Singh, J. Kalita and S.S. Singh, *Inorg. Chim. Acta*, **439**, 164 (2016); https://doi.org/10.1016/j.ica.2015.10.012
65. N.H. Nasaruddin, S.N. Ahmad, S.S. Sirat, T.K. Wai, N.A. Zakaria and H. Bahron, *J. Mol. Struct.*, **1232**, 130066 (2021); https://doi.org/10.1016/j.molstruc.2021.130066
66. A.J. Stasyuk, M. Solà and A.A. Voityuk, *Sci. Rep.*, **8**, 2882 (2018); https://doi.org/10.1038/s41598-018-21240-0